**ADVANCED
SCIENCE NEWS**

www.advancedsciencenews.com

**ADVANCED
ENERGY
MATERIALS**

www.advenergymat.de

COMMUNICATION

Layered VS$_2$ Nanosheet-Based Aqueous Zn Ion Battery Cathode

Pan He, Mengyu Yan, Guobin Zhang, Ruimin Sun, Lineng Chen, Qinyou An,* and Liqiang Mai*

The continuous researches of energy-storage devices have gained considerable attention in our world which results from the increased development of new-type energy caused by energy crisis and environmental pollution.[1–3] In the past several decades, lithium ion batteries have been widely explored and applied to various fields as they deliver higher energy density compared to other secondary batteries.[4,5] Nevertheless, the processing cost, complicated issues of safety, the limited lithium resources as well as some environmental issues lead to an urgent challenge for exploring new energy storage system.[6,7] The rechargeable aqueous batteries, such as aqueous sodium-ion batteries and aqueous Zn ion batteries (ZIBs) have received incremental attention because of cost effectiveness and material abundance.[8–16] There is interest in aqueous ZIBs due to the safety, low cost, abundance of Zn source, and utilizing divalent cations to increase charge-storage capabilities. However, existing aqueous ZIBs are far from achieving the goals of excellent performances demanded by the ever increasing energy consumption. It's hard to find cathode materials suitable for the reversible intercalation/deintercalation of Zn ions (or their solvation sheath in electrolyte), which limits the developmen of ZIBs.[16] The previous explorations of the cathode material mostly focus on manganese dioxide (MnO$_2$) and Prussian blue analogues, whereas, the former suffers a poor rate performance and a rapid capacity fading, while the latter delivers limited capacities (about 50 mA h g^{-1}).[17–22] Recently, Nazar and co-workers reported a high-capacity and long-life aqueous rechargeable zinc battery, composing of a Zn$_{0.25}$V$_2$O$_5$·nH$_2$O nanobelts cathode, 1 M ZnSO$_4$ electrolyte, and a zinc anode.[23] The work indicates that the layered structure materials show great potential for the cathode of ZIBs.

During the past decades, layered transition-metal dichalcogenides (TMDs), such as MoS$_2$, WS$_2$, and VS$_2$ have received significant attentions in a variety of fields for their outstanding characteristic (graphene-like layered structure, direct bandgap, and fast ion diffusion).[24–26] These properties make TMDs potential candidates for battery electrode materials. When applied as the electrode materials for lithium/sodium ion battery, some excellent studies have been reported.[27–29] Also, this class of materials show great potential for the insertion/extraction of multivalent ions (Zn^{2+}, Mg^{2+}, Al^{3+}) owing to the characteristic of large layer spacing and high conductivity. Among all the TMDs, VS$_2$ is a typical family member of TMDs with hexagonal system, which shows similar crystal structure to that of graphite lamellar with an interlayer spacing of 5.76 Å.[25,30] There is a vanadium layer between two sulfur layers to form a kind of sandwich structure. In VS$_2$ crystal structure, each V atom is arranged around six S atoms and connected with S atoms with covalent bonds. The interlayer spacing of VS$_2$ is so large that enables the convenient insertion/extraction of lithium ions (0.69 Å), sodium ions (1.02 Å), zinc ions (0.74 Å) or their solvation sheath in electrolyte. However, to the best of our knowledge, there is no report about VS$_2$ as the electrode materials for ZIBs.

Herein, the VS$_2$ nanosheets are synthesized via a facile hydrothermal reaction (Supporting Information), which deliver a high capacity of 190.3 mA h g^{-1} at a current density of 0.05 A g^{-1} and exhibit long-term cyclic stability as the cathode for ZIBs. The electrochemical reaction mechanism of such VS$_2$ electrodes is further investigated systematically through a series of measurements including ex situ X-ray diffraction (XRD), ex situ X-ray photoelectron spectroscopy (XPS), in situ Raman, ex situ transmission electron microscopy (TEM). A reversible insertion/extraction process can be observed from all aspects. Both the ex situ TEM and ex situ XRD results demonstrate that the interlayer space of VS$_2$ can self adapt to the intercalation of Zn^{2+} with an expansion along the *c*-axis (only 1.73%) and a slightly shrink along the *a*- and *b*-axes, which plays a key role in the realization of long-life ZIBs. All the above evidences reveal that the VS$_2$ is a promising cathode material with high capacity and good cyclic stability for ZIBs.

The crystal structure of the as-prepared VS$_2$ is tested by XRD. All characteristic peaks are in accordance with the standard card of VS$_2$ (JCPDS NO. 01-089-1640) (**Figure 1**a). The Raman spectrum of the VS$_2$ in the range of 100–1100 cm^{-1} is shown in Figure 1b. Six peaks located at 140.4, 192.0, 282.0, 406.6, 687.8, and 993.2 cm^{-1} are observed, which correspond to the rocking and stretching vibrations of V–S bonds or their combination.[25] The morphology and microstructures of as-prepared VS$_2$ are investigated by field emission scanning electron microscopy (SEM) and high-resolution TEM (HRTEM). As shown in Figure 1c, The VS$_2$ flowers are assembled by nanosheets with a diameter of 5–8 µm and a thickness of 50–100 nm. The *d*-spacing calculated from selected area electron diffraction (SAED) patterns are 2.89 and 1.64 Å (**Figure 2**f), which match the *d*-spacing values of (002) and (110) crystal planes of VS$_2$, respectively. TEM and corresponding HRTEM images in Figure 2e show VS$_2$ nanosheets with a *d*-spacing of ≈5.76 Å,

P. He, Dr. M. Yan, G. Zhang, R. Sun, L. Chen,
Prof. Q. An, Prof. L. Mai
State Key Laboratory of Advanced Technology
for Materials Synthesis and Processing
Wuhan University of Technology
Wuhan 430070, China
E-mail: anqinyou86@whut.edu.cn;
mlq518@whut.edu.cn

**ADVANCED
ENERGY
MATERIALS**
www.advenergymat.de

**ADVANCED
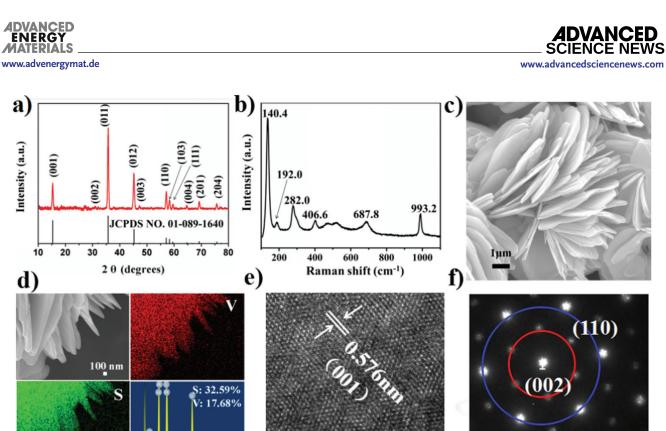SCIENCE NEWS**
www.advancedsciencenews.com

COMMUNICATION

Figure 1. The characterization of layered VS_2: a) XRD pattern, b) Raman spectra, c) SEM, d) SEM–EDX, e) HR-TEM image, and f) SAED.

which corresponds to the (001) plane of monoclinic phase of VS_2. The energy dispersive X-ray spectroscopy (EDX) elemental mapping is used to determine the stoichiometry of V and S. As shown in Figure 1d (SEM–EDX) and Figure S1 (TEM–EDX; Supporting Information), the results clearly indicate that V and S elements are distributed homogeneously with the ratio of about 1: 2. Furthermore, we also investigate the growth process of VS_2 nanosheets by controlling the reaction time (Figure S2, Supporting Information). No specific morphology is observed when simply mixing the NH_4VO_3 and thioacetamide (TAA) before hydrothermal treatment. Rose-like microflowers assembled by nanosheets with diameter of 4–6 µm begin to emerge with the hydrothermal reaction time from 4 to 8 h. Then, the microflowers stretch out bit by bit to form laminated sheet structure.

In order to investigate the electrochemical performances of VS_2, CR2016 coin-type cells are fabricated. Figure 2a,b show the charge and discharge curves and rate capability of VS_2 cycling in the voltage range of 0.4–1.0 V at the current density from 0.1 to 2.0 A g^{-1}. The charge and discharge curves at a current density of 0.1 A g^{-1} keep stable plateaus, which locate at 0.72/0.76 V and 0.63/0.68 V, respectively (Figure S3, Supporting Information). The discharge capacities are 190.3, 159.1, 145.3, 136.8, 121.5, and 115.5 mA g^{-1} at 0.05, 0.1, 0.2, 0.5, 1.0, and 2.0 A g^{-1}, respectively. The cycling performance is further tested at a current density of 0.5 A g^{-1}. The charge and discharge curves of VS_2 at different cycles are shown in Figure S4 (Supporting Information). The charge and discharge plateaus are still clearly visible even at 200th cycles, indicating the high reversibility of the reactions. The cycling data in Figure 2c

shows that the initial discharge capacity is 112.3 mA h g^{-1}. The capacities increase gradually in the first few cycles, which can be related to the gradual activation of the electrode.[34] After 200 cycles, the discharge capacity is 110.9 mA h g^{-1} (98.0% of the value in the first cycle) and the coulombic efficiency approaches to 100% in all cycles.

To further understand the electrochemical kinetics of VS_2 nanosheets electrode, cyclic voltammetly (CV) measurements are carried out at various scan rates from 0.1 to 1.0 mV s^{-1}. At 0.1 mV s^{-1} (Figure S5, Supporting Information), there are two pairs reduction/oxidation peaks located at 0.58/0.63 and 0.72/0.75 V, which are in accordance with plateaus of the discharge/charge curves (Figure S4, Supporting Information). With the increase of scan rates from 0.1 to 1.0 mV s^{-1}, the CV curves display similar shapes and gradual broaden peaks can be observed. A general approach for analyzing the electrochemical kinetics processes, based on the scan rate test data, is described as the following equation[31,32]

$$i = av^b \tag{1}$$

where a and b are adjustable parameters, i is the current (A), and v is the scan rate (V s^{-1}). Generally, the coefficient b varies in the range 0.5–1.0 and the b-value of 0.5 represents a diffusion-limmited process, while 1.0 indicates a capacitive process. The relationship between $\log(i)$ (at every peak current) and $\log(v)$ are shown in Figure 2e. The b-value determined by the slopes of the four redox peaks are 0.89, 0.75, 0.92, and 0.78, which implies that the capacity of VS_2 is little influenced by the diffusion process. Furthermore, the relationship $i = av$b can be
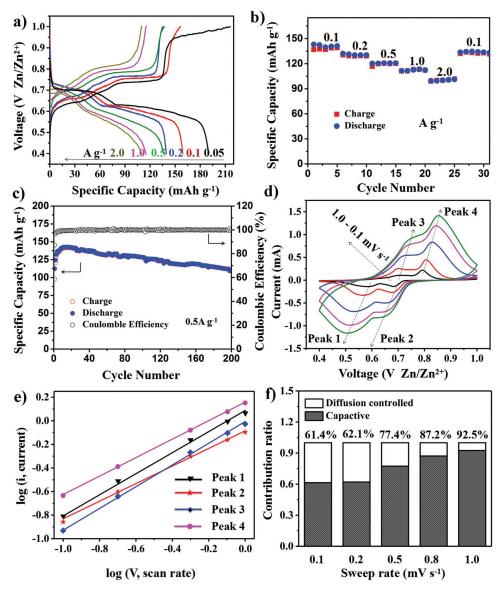
Figure 2. Electrochemical performances of Zn/VS$_2$ batteries cycling in a range of 0.4–1.0 V. a) Charge and discharge curves at the current density from 0.05 to 2.0 A g^{-1}. b) Rate capability. c) Long-term cyclic properties at a current density of 0.5 A g^{-1}. d) CV curves at different scan rates. e) Log(i) versus log(v) plots at specific peak currents. f) The contribution ratio of the capacitive capacities and diffusion-limited capacities.

divided into two parts including capacitive (k_1v) and diffusion-limited effects ($k_2v^{1/2}$), as described below[33,34]

$$i = k_1v + k_2v^{1/2} \qquad (2)$$

or

$$i/v^{1/2} = k_1v^{1/2} + k_2 \qquad (3)$$

At a particular voltage, the k_1-value characterizes the capacitive and k_2-value corresponds to diffusion limited. For instance, ≈62.1% of the total current, namely the capacity, is contributed by capacitive properties in nature at a scan rate of 0.2 mV s^{-1} (Figure S5, Supporting Information). Also, contribution ratios of capacitive mechanisms at other scan rates are calculated, as shown in Figure 2f. The results show that the capacitive

contribution holds dominant position in the total capacity and the contribution ratios of capacitive gradually increase with improvement of the scan rate.

The ex situ XRD, in situ Raman, ex situ SAED, ex situ XPS, and ex situ HRTEM are applied to explore the storage mechanism of Zn/VS$_2$ systems. **Figure 3**a displays the XRD patterns of the VS$_2$ electrode at different charge/discharge states of the third cycle. Generally, the intensity and position of XRD peaks remain unchanged except a characteristic peak located at 15.4°, which shift visibly during the charge/discharge processes. In detail, when discharged to 0.8 V (state I to state II in Figure 3a), there is no obvious change of the typical peaks. The peak of 15.4° gradually decreases slightly from state II to VI, resulting from the increase of the interlayer spacing(d_{001}), which is caused by the insertion of Zn ion during the discharge process. On the contrary, the d_{001} gradually decreases from state VI to X,

**ADVANCED
ENERGY
MATERIALS**
www.advenergymat.de

**ADVANCED
SCIENCE NEWS**
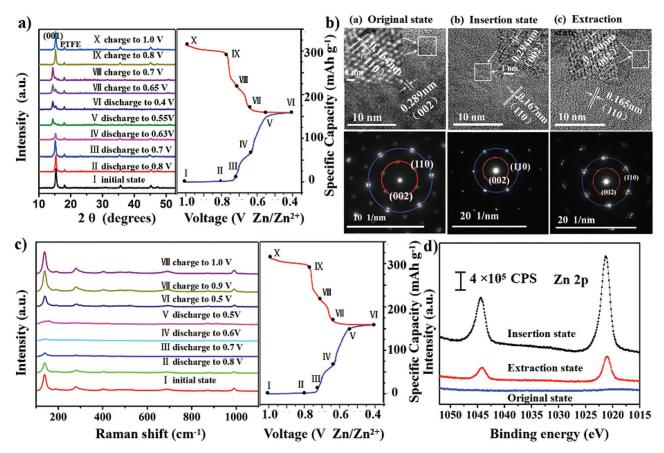www.advancedsciencenews.com

COMMUNICATION

Figure 3. a) Ex situ XRD patterns of VS_2 collected at various states. b) HR-TEM images and SAED patterns. c) In situ Raman spectra of VS_2 electrode at a scan rate of 2.0 mV s^{-1} in the voltage range of 0.4–1.0 V. d) Zn 2p core level spectra of VS_2 electrodes in original, insertion, and extraction states.

resulting in the decrease of the characteristic peak located at 15.4° during the charge processes. When charged to 1.0 V, the peaks return to their original values, indicating a completely reversible structure evolution. The HRTEM and SAED display a slight change of the lattice spacing of (002) during the de/intercalation of Zn^{2+} (Figure 3b). When discharged to 0.4 V, the lattice spacing of (002) increases by 1.73% than the original state, which confirms the intercalation reaction mechanism and fits well with the ex situ XRD results.

Figure 3c shows the in situ Raman spectra of VS_2 at different applied potential during the CV test at a scan rate of 2.0 mV s^{-1}. Obvious changes of the five main peaks located at 140.4, 282.0, 406.6, 687.8 and 993.2 cm^{-1} are observed during the charge/discharge processes. During the discharge progress from 1.0 to 0.4 V, the bands at 140.4, 282.0, 406.6, 687.8, and 993.2 cm^{-1} become weaker and broader, corresponding to the intercalation of cations between the layers of VS_2. On the contrary, as the potential increase from 0.4 to 1.0 V, the intensity of these peaks gradually strengthen and return to the original state, which are caused by the extraction of Zn^{2+} from the layers of VS_2. Zn 2p core level spectra of VS_2 electrodes in original, insertion (at 0.4 V), and extraction (at 1.0 V) states are shown in Figure 3d. The intensity of Zn 2p from extraction states is far below the insertion states, which confirms the insertion/extraction of Zn^{2+} into/from the interlamination of VS_2.

In consequence, the mechanism of Zn/VS_2 systems is illustrated in **Figure 4**, the electrochemical reaction in the two electrodes can be summarized as below

In the cathode

$$VS_2 + 0.09Zn^{2+} + 0.18e^- \leftrightarrow Zn_{0.09}VS_2 \tag{4}$$

$$Zn_{0.09}VS_2 + 0.14Zn^{2+} + 0.28e^- \leftrightarrow Zn_{0.23}VS_2 \tag{5}$$

In the anode

$$Zn^{2+} + 2e^- \leftrightarrow Zn \tag{6}$$

During the discharge processes, Zn^{2+} ions are intercalated into the layers of VS_2, which can be divided into two steps. The content of Zn^{2+} is calculated according to the discharge curve cycled at a current density of 0.05 A g^{-1} (Figure S6, Supporting Information). In the first step, the phase transition from VS_2 to conductive $Zn_{0.09}VS_2$ appears in the voltage range of 0.82–0.65 V, promoting a highly reversible intercalation reaction.[34] A following phase change from $Zn_{0.09}VS_2$ to $Zn_{0.23}VS_2$ occurs in the voltage range of 0.65–0.45 V, which provides a immense contribution of capacities. In the case of charge processes, Zn^{2+} ion deintercalated from $Zn_{0.23}VS_2$ to form the VS_2 phase gradually.

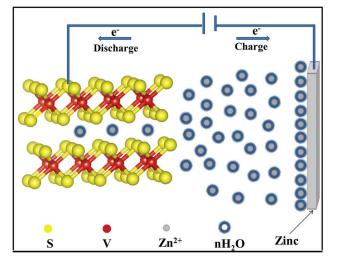**Figure 4.** Schematic illustration of the operation mechanism of Zn/VS_2 batteries

In summary, aqueous Zn/VS_2 batteries are designed and constructed for the first time. The VS_2 electrode delivers a high capacity of 190.3 mA h g^{-1} at a current density of 0.05 A g^{-1} and the energy density is 123 W h kg^{-1} based on the all active electrode materials, which is much higher than traditional lead–acid and nickel–chromium batteries. What is more, the battery also exhibits long-term cyclic stability (capacity retention ratio is 98.0% after 200 cycles) and good rate performance. The intercalation reaction mechanism has also been proved by ex situ XRD, ex situ TEM, ex situ XPS, and in situ Raman for the first time. The design of Zn/VS_2 battery composed of a VS_2 cathode, a zinc anode, and a mild $ZnSO_4$ aqueous electrolyte may have a significant impact on large-scale energy storage due to its low cost, safety, and environmentally friendly. Also, the development of layered transition-metal dichalcogenides as cathodes for aqueous ZIBs may bring intensive interest to later researches.

Supporting Information

Supporting Information is available from the Wiley Online Library or from the author.

Acknowledgements

[1] B. Dunn, H. Kamath, J.-M. Tarascon, *Science* **2011**, *334*, 928.
[2] D. Larcher, J.-M. Tarascon, *Nat. Chem.* **2015**, *7*, 19.
[3] P. Yang, J.-M. Tarascon, *Nat. Mater.* **2012**, *11*, 560.
[4] L. Q. Mai, Q. L. Wei, Q. Y. An, X. C. Tian, Y. L. Zhao, X. Xu, L. Xu, L. Chang, Q. J. Zhang, *Adv. Mater.* **2013**, *25*, 2969.
[5] J. Bai, X. G. Li, G. Z. Liu, Y. T. Qian, S. L. Xiong, *Adv. Funct. Mater.* **2014**, *24*, 3012.
[6] J. B. Goodenough, Y. Kim, *Chem. Mater.* **2009**, *22*, 587.
[7] V. Etacheri, R. Marom, E. Ran, G. Salitra, D. Aurbach, *Energy Environ. Sci.* **2011**, *4*, 3243.
[8] M. Pasta, C. D. Wessells, N. Liu, J. Nelson, M. T. McDowell, R. A. Huggins, M. F. Toney, Y. Cui, *Nat. Commun.* **2014**, *5*, 155.
[9] Y. Wang, J. Liu, B. Lee, R. Qiao, Z. Yang, S. Xu, X. Yu, L. Gu, Y. S. Hu, W. Yang, K. Kang, H. Li, X. Q. Yang, L. Chen, X. Huang, *Nat. Commun.* **2015**, *6*, 6401.
[10] Z. Li, D. Young, K. Xiang, W. C. Carter, Y. M. Chiang, *Adv. Energy Mater.* **2013**, *3*, 290.
[11] Y. H. Jung, C. H. Lim, J. H. Kim, D. K. Kim, *RSC Adv.* **2014**, *4*, 9799.
[12] H. B. Zhao, C. J. Hu, H. W. Cheng, J. H. Fang, Y. P. Xie, W. Y. Fang, T. N. Doan, T. K. Hoang, J. Q. Xu, P. Chen, *Sci. Rep.* **2016**, *6*, 25809.
[13] Y. Liu, Y. Qiao, W. X. Zhang, H. H. Xu, Z. Li, Y. Shen, L. X. Yuan, X. L. Hu, X. Dai, Y. H. Huang, *Nano Energy* **2014**, *5*, 97.
[14] C. Deng, S. Zhang, Z. Dong, Y. Shang, *Nano Energy* **2014**, *4*, 49.
[15] C. J. Xu, B. H. Li, H. D. Du, F. Y. Kang, *Angew. Chem., Int. Ed.* **2012**, *51*, 933.
[16] H. L. Pan, Y. Y. Shao, P. F. Yan, Y. W. Cheng, K. S. Han, Z. M. Nie, C. M. Wang, J. H. Yang, X. L. Li, P. Bhattacharya, K. T. Mueller, J. Liu, *Nat. Energy* **2016**, *1*, 16039.
[17] L. Y. Zhang, L. Chen, X. F. Zhou, Z. P. Liu, *Adv. Energy Mater.* **2015**, *5*, 1400930.
[18] Z. Liu, G. Pulletikurthi, F. Endres, *ASC Appl. Mater. Interfaces* **2016**, *8*, 12158.
[19] J. Lee, J. B. Ju, W. I. Cho, B. W. Cho, S. H. Oh, *Electrochim. Acta* **2013**, *112*, 138.
[20] M. H. Alfaruqi, V. Mathew, J. Gim, S. Kim, J. Song, J. P. Baboo, H. C. Sun, J. Kim, *Chem. Mater.* **2015**, *27*, 3609.
[21] M. H. Alfaruqi, J. Gim, S. Kim, J. Song, D. T. Pham, J. Jo, Z. Xiu, V. Mathew, J. Kim, *Electrochem. Commun.* **2015**, *60*, 121.
[22] D. Xu, B. Li, C. Wei, Y.-B. He, H. Du, X. Chu, X. Qin, Q.-H. Yang, F. Kang, *Electrochim. Acta* **2014**, *133*, 254.
[23] D. Kundu, B. D. Adams, V. Duffort, S. H. Vajargah, L. F. Nazar, *Nat. Energy* **2016**, *1*, 16119.
[24] S. H. Choi, Y. C. Kang, *Nanoscale* **2015**, *7*, 3965.
[25] J. Feng, X. Sun, C. Wu, L. Peng, C. Lin, S. Hu, J. Yang, Y. Xie, *J. Am. Chem. Soc.* **2011**, *133*, 17832.
[26] Y. Li, H. Wang, L. Xie, Y. Liang, G. Hong, H. Dai, *J. Am. Chem. Soc.* **2011**, *133*, 7296.
[27] H. Hwang, H. Kim, J. Cho, *Nano Lett.* **2011**, *11*, 4826.
[28] Z. Hu, L. X. Wang, K. Zhang, J. B. Wang, F. Y. Cheng, Z. L. Tao, J. Chen, *Angew. Chem., Int. Ed.* **2014**, *126*, 13008.
[29] C. S. Rout, B-H. Kim, X. D. Xu, J. U. Yang, H. Y. Jeong, D. Odkhuu, N. Park, J. Cho, H. S. Shin, *J. Am. Chem. Soc.* **2013**, *135*, 8720.
[30] J. Feng, L. Peng, C. Wu, X. Sun, S. Hu, C. Lin, J. Dai, J. Yang, Y. Xie, *Adv. Mater.* **2012**, *24*, 1969.
[31] T. Brezesinski, J. Wang, S. H. Tolbert, B. Dunn, *Nat. Mater.* **2010**, *9*, 146.
[32] J. Wang, J. Polleux, A. James Lim, B. Dunn, *J. Phys. Chem. C* **2007**, *111*, 14925.
[33] P. Simon, Y. Gogotsi, B. Dunn, *Science* **2014**, *343*, 1210.
[34] K. Zhang, Z. Hu, X. Liu, Z. Tao, J. Chen, *Adv. Mater.* **2015**, *27*, 3305.